arXiv:1410.3960

Cosmological Models and Gamma-Ray Bursts Calibrated by Using Padé Method

Jing Liu * and Hao Wei †
School of Physics, Beijing Institute of Technology, Beijing 100081, China

arXiv:1410.3960v3 [astro-ph.CO] 8 Nov 2015

ABSTRACT

Gamma-ray bursts (GRBs) are among the most powerful sources in the universe. In the recent years, GRBs have been proposed as a complementary probe to type Ia supernovae (SNIa). However, as is well known, there is a circularity problem in the use of GRBs to study cosmology. In this work, based on the Padé approximant, we propose a new cosmology-independent method to calibrate GRBs. We consider a sample consisting of 138 long Swift GRBs and obtain 79 calibrated long GRBs at high-redshift $z > 1.4$ (named Mayflower sample) which can be used to constrain cosmological models without the circularity problem. Then, we consider the constraints on several cosmological models with these 79 calibrated GRBs and other observational data. We show that GRBs are competent to be a complementary probe to the other well-established cosmological observations.

PACS numbers: 98.80.Es, 95.36.+x, 98.70.Rz, 98.80.Cq

* email address: liujing5972@163.com
† Corresponding author; email address: haowei@bit.edu.cn

I. INTRODUCTION

Based on the observations of type Ia supernovae (SNIa), the current acceleration of the universe was firstly discovered in 1998 [1]. This great discovery hints the existence of a new component with negative pressure called dark energy, or a modification to general relativity on the cosmological scale. In order to understand the cosmic acceleration, astronomers have made much effort on the cosmological observations. Besides SNIa, as is well known, there are other well-established cosmological observations such as baryon acoustic oscillations (BAO) and cosmic microwave background (CMB).

In the recent years, Gamma-Ray Bursts (GRBs) [2–5, 57] have been proposed as a complementary probe to SNIa. Their high energy photons in the gamma-ray band are almost immune to dust extinction, and hence they have been observed up to redshift $z \sim 8-9$ [6, 7], well beyond the observed redshift range of SNIa, namely $z < 2$ [8]. Thus, we might use GRBs to explore the early universe in the high redshift range which is difficult to access by other cosmological probes. To our knowledge, using GRBs to constrain the cosmological models was firstly performed by Dai *et al.* [9]. However, there is a so-called "circularity problem" [2] in the direct use of GRBs, mainly due to the lack of a set of low-redshift GRBs at $z < 0.1$ which are cosmology-independent. To calibrate the empirical GRB luminosity relations, one should assume a particular cosmological model with some model parameters *a priori*. Therefore, when one uses these "calibrated" GRBs (which are actually cosmology-dependent) to constrain cosmological models, the circularity problem appears. To alleviate the circularity problem, some statistical methods were proposed, including the scatter method [10], the luminosity distance method [10, 11], the Bayesian method [12], and so on. However, they still cannot solve the circularity problem completely.

Up to date, in the literature there are several cosmology-independent methods to avoid the circularity problem. For example, Li *et al.* [13] proposed that one can treat the parameters involved in the empirical GRB correlation relation as free parameters, and determine them simultaneously with the cosmological model parameters by using GRBs data together with other observational data. However, for any given cosmological model, this method can always obtain some parameters for the cosmological model and the empirical GRB luminosity relation. In this sense, any cosmological model is "viable" (except for a few obviously absurd models), and hence this method cannot be used to rule out any cosmological model. So, it is not a satisfactory method to solve the circularity problem completely. A completely cosmology-independent method was proposed by Liang *et al.* [14]. The key idea is using distance ladder to calibrate GRBs. Similar to calibrating SNIa as secondary standard candles by using Cepheid variables which are primary standard candles, we can also calibrate GRBs as standard candles with a large amount of SNIa. Liang *et al.* [14] proposed to divide GRBs into two groups, whose redshifts are $z < 1.4$ and $z \geq 1.4$, respectively. Using a cubic interpolation method, one can obtain the distance modulus of a GRB at a given low-redshift $z < 1.4$ by interpolating from the Hubble diagrim of SNIa. Since the distance moduli of SNIa are obtained directly from observations, this method is completely cosmology-independent. We can calibrate the empirical GRB luminosity relations with these low-redshift GRBs at $z < 1.4$, and then derive the distance moduli of the high-redshift GRBs at $z \geq 1.4$ by using the calibrated empirical GRB luminosity relations. Obviously, the calibrated high-redshift GRBs can be used to constrain cosmological models without the circularity problem. In [15, 16], Wei *et al.* have further developed this method. They considered a sample of 109 GRBs, and obtained 59 calibrated high-redshift GRBs (named Hymnium sample) [16] which can be used to constrain cosmological models. It is worth noting that almost at the same time, Kodama *et al.* [17] proposed a similar method using also the idea of distance ladder. Instead of the cubic interpolation method used in [14–16], Kodama *et al.* [17] found an completely empirical formula for the luminosity distance of SNIa at redshift $0.359 < z < 1.755$, namely

$$\frac{d_L}{10^{27}\,\mathrm{cm}} = 14.57 \times z^{1.02} + 7.16 \times z^{1.76}\,. \tag{1}$$

Then, similar to [14–16], Kodama *et al.* [17] calibrated the empirical GRB luminosity relations with these low-redshift GRBs at $z \leq 1.755$, and then derive the distance moduli of the high-redshift GRBs at $z > 1.755$ by using the calibrated empirical GRB luminosity relations. Obviously, this method has a fatal drawback. As is also admitted by them, the empirical formula in Eq. (1) was written purely by hand without any theoretical foundation. Thus, this method has not been widely used in the literature. On the other hand, Capozziello *et al.* [18] considered a cosmography method (see also e.g. [19]). They expanded the luminosity distance d_L by using the Taylor series up to high order in redshift z, whose

coefficients are characterized by the cosmographic parameters [58], namely the Hubble constant H_0, deceleration parameter q_0, jerk j_0, snap s_0 and lerk l_0. Then, they fitted this luminosity distance d_L to SNIa dataset, and obtained the best-fit cosmographic parameters with 1σ uncertainty. So, the luminosity distance of GRBs can be derived from the d_L expansion with the cosmographic parameters calibrated by SNIa. Obviously, this method is also cosmology-independent. However, it is well known that the Taylor series converges only for small z, and it might diverge at higher redshifts (especially when $z \gtrsim 1$). This shortcoming cannot be completely cured by replacing the redshift z with the so-called y-shift $y \equiv z/(1+z)$, because the error of Taylor approximation throwing away the higher order terms will become unacceptably large when y is close to 1 (say, when $z > 9$). Unlike the above methods, Wang [20] considered the calibration of GRBs by using the data of GRBs internally, without invoking any external datasets (e.g. SNIa). Based on this method, considering the sample of 109 GRBs given by Wei [16], Xu [21] derived five data points of distance measurements which do not depend on any cosmological models. However, the method of Wang [20] is still under a slight suspicion that it is not so model-independent actually. In this method, when one determines the statistical errors of correlation parameters and the systematic error, a particular ΛCDM model with $\Omega_{m0} = 0.27$ was assumed, although they claimed that the correlation parameters themselves do not depend on this assumed ΛCDM model [20, 21]. On the other hand, in this method the absolute magnitude of GRBs is unknown, only the slopes of GRBs correlations can be used as cosmological constraints. As a result, it is shown in e.g. [21] that the constraints on cosmological models using this method is looser than the one of [16] which uses the method proposed by Liang *et al.* [14]. In fact, several further potential drawbacks of the method of Wang [20] were listed in, for example, the last section of [21].

In the present work, we try to further develop the cosmology-independent method to calibrate GRBs. Inspired by the methods proposed by Liang *et al.* [14], Kodama *et al.* [17], and Capozziello *et al.* [18], we propose a new method engrafting the advantages of these three methods without their drawbacks. We keep the key idea of distance ladder and the main framework of the method used in e.g. [14–16], but change the method to obtain the distance moduli (or luminosity distances equivalently) of the low-redshift GRBs at $z < 1.4$. Instead of the purely empirical formula for the luminosity distance of SNIa in Eq. (1) [17], or the Taylor expansion of the luminosity distance of SNIa [18], we consider the Padé approximant, which can be regarded as a generalization of Taylor polynomial [22, 23]. In mathematics, a Padé approximant is the best approximation of a function by a rational function of given order [22]. In fact, the Padé approximant often gives better approximation of the function than truncating its Taylor series, and it may still work where the Taylor series does not converge [22]. For any function $f(x)$, its corresponding Padé approximant of order (m, n) is given by the rational function [22, 23]

$$f(x) = \frac{\alpha_0 + \alpha_1 x + \cdots + \alpha_m x^m}{1 + \beta_1 x + \cdots + \beta_n x^n}\,, \tag{2}$$

where m and n are both non-negative integers; α_i and β_i are all constants. Obviously, it reduces to the Taylor polynomial when all $\beta_i = 0$. It is worth noting that if we express the luminosity distance of SNIa at low redshift $z < 1.4$ with the Padé approximant, it is well motivated from the theoretical point of view, unlike the empirical formula in Eq. (1) purely written by hand [17]. As mentioned above, the Padé approximant can also avoid the divergence of Taylor polynomial at high redshift, unlike the case of cosmography method [18].

In this work, we consider a sample consisting of 138 long Swift GRBs (see e.g. [60] for Swift mission). It includes 109 long GRBs adopted directly from [16], which have 50 low-redshift GRBs at $z < 1.4$ and 59 high-redshift GRBs at $z > 1.4$. In addition, we adopt other 29 long GRBs from [24], which include 9 low-redshift GRBs (050126A, 050223, 050803, 060904B, 100621A, 100816A, 101219B, 070508, 100414A) and 20 high-redshift GRBs (100814A, 110213A, 100906A, 081203A, 100728B, 080804, 110205A, 070110, 060714, 060607A, 050908, 061222B, 060906, 060605, 060210, 050505, 060223A, 060510B, 060522, 050814). In total, we have 59 low-redshift GRBs at $z < 1.4$ and 79 high-redshift GRBs at $z > 1.4$.

The rest of this paper is organized as followings. In Sec. II, we calibrate 138 GRBs with Union2.1 SNIa dataset using the method of Padé approximant. We obtain 79 calibrated GRBs at high redshift $z > 1.4$ (named Mayflower sample) which can be used to constrain cosmological models without the circularity problem. In Sec. III, we consider the constraints on several cosmological models with these 79 calibrated GRBs and other observational data. In Sec. IV, the conclusion and discussions are given.

$(m,\ n)$	(1, 1)	(1, 2)	(1, 3)	(1, 4)	(2, 1)	(2, 2)	(2, 3)	(2, 4)
χ^2_{min}	1626.99	738.582	608.276	576.214	719.261	571.932	561.947	561.032
k	3	4	5	6	4	5	6	7
χ^2_{min}/dof	2.8197	1.2823	1.0579	1.0039	1.2487	0.9950	0.979	0.9791
ΔBIC	1046.06	164.015	40.072	14.373	144.694	3.728	0.106	5.554
ΔAIC	1059.15	172.741	44.435	14.373	153.42	8.091	0.106	1.191
$(m,\ n)$	(3, 1)	(3, 2)	(3, 3)	(3, 4)	(4, 1)	(4, 2)	(4, 3)	(4, 4)
χ^2_{min}	601.157	561.841	560.891	560.82	573.314	561.006	560.82	560.82
k	5	6	7	8	6	7	8	9
χ^2_{min}/dof	1.0455	0.9788	0.9789	0.9805	0.9988	0.9791	0.9805	0.9822
ΔBIC	32.953	0	5.413	11.705	11.473	5.528	11.705	18.068
ΔAIC	37.316	0	1.05	2.979	11.473	1.165	2.979	4.979

TABLE I: Comparing various Padé approximants up to order (4, 4). See the text for details.

II. CALIBRATING GRBS WITH THE METHOD OF PADÉ APPROXIMANT

In this section, we calibrate 138 GRBs with Union2.1 SNIa dataset [25] (which consists of 580 SNIa) using the method of Padé approximant. The first step is to find a formula for the distance moduli (or luminosity distances equivalently) of these 580 Union2.1 SNIa. Instead of purely empirical formula [17] or Taylor expansion [18], we consider the Padé approximant given in Eq. (2) which is well motivated from the theoretical point of view as mentioned above. Now, the question is how to choose the order $(m,\ n)$ of Padé approximant. If the order is too low, the error of Padé approximant will be unacceptably large. If the order is too high, the number of free coefficients are too much and the uncertainties will be large. To find the suitable order $(m,\ n)$, we test all the corresponding Padé approximants up to order (4, 4) one by one. For each Padé approximant of given order, we fit the distance moduli in the expression of Padé approximant to the real Union2.1 SNIa dataset, and minimize the corresponding χ^2, namely

$$\chi^2 = \sum_i \frac{\left[\mu_{obs}(z_i) - \mu_{pade}(z_i)\right]^2}{\sigma_i^2}\,, \tag{3}$$

where σ is the corresponding 1σ error. Then, we compare all these 16 Padé approximants up to order (4, 4). A conventional criterion for comparison in the literature is χ^2_{min}/dof, in which the degree of freedom $dof = N-k$, whereas N and k are the number of data points and the number of free parameters, respectively. In addition, we also consider other two criterions used extensively in the literature, namely the so-called Bayesian Information Criterion (BIC) and Akaike Information Criterion (AIC). The BIC is defined by [53]

$$\mathrm{BIC} = -2\ln\mathcal{L}_{max} + k\ln N\,, \tag{4}$$

where $\mathcal{L}_{max}$ is the maximum likelihood. In the Gaussian cases, $\chi^2_{min} = -2\ln\mathcal{L}_{max}$. So, the difference in BIC between two fits is given by $\Delta\mathrm{BIC} = \Delta\chi^2_{min} + \Delta k\ln N$. The AIC is defined by [54]

$$\mathrm{AIC} = -2\ln\mathcal{L}_{max} + 2k\,. \tag{5}$$

Accordingly, the difference in AIC between two fits is given by $\Delta\mathrm{AIC} = \Delta\chi^2_{min} + 2\Delta k$. We present the results in Table I. Notice that the Padé approximant of order (3, 2) has been chosen to be the fiducial one when we calculate ΔBIC and ΔAIC. From Table I, it is easy to see that the Padé approximant of order (3, 2) is the best. So, we express the distance moduli in Padé approximant of order (3, 2), namely

$$\mu_{pade}(z) = \frac{\alpha_0 + \alpha_1 z + \alpha_2 z^2 + \alpha_3 z^3}{1 + \beta_1 z + \beta_2 z^2}\,. \tag{6}$$

We fit this formula for the distance moduli to the real 580 Union2.1 SNIa dataset. By minimizing the corresponding χ^2 in Eq. (3), we find that the best-fit coefficients (with 1σ errors) are given by $\alpha_0 = 30.1297 \pm 0.9086$, $\alpha_1 = 2654.46 \pm 898.233$, $\alpha_2 = 10740.4 \pm 6173.28$, $\alpha_3 = 351.476 \pm 262.753$, $\beta_1 = 71.3026 \pm 25.3371$, $\beta_2 = 239.978 \pm 140.868$, while $\chi^2_{min} = 561.841$. The corresponding covariance matrix [26] (see also e.g. [27, 28]) is given by

$$\begin{pmatrix} 0.825595685565 & -802.86374851 & -5283.1838241 & -212.71322979 & -22.600394329 & -120.172829002 \\ -802.86374851 & 806822.199728 & 5458365.5695 & 223635.10205 & 22757.10276006 & 124325.358406 \\ -5283.1838241 & 5458365.5695 & 38109346.82922 & 1600878.89393 & 154260.002287 & 869566.838689 \\ -212.71322979 & 223635.10205 & 1600878.89393 & 69039.099861 & 6328.7278164 & 36588.879649 \\ -22.600394329 & 22757.10276006 & 154260.002287 & 6328.7278164 & 641.968817 & 3513.94073660 \\ -120.172829002 & 124325.358406 & 869566.838689 & 36588.879649 & 3513.94073660 & 19843.704035 \end{pmatrix} \tag{7}$$

In Fig. 1, we present the Hubble diagram of 580 Union2.1 SNIa and the distance moduli expressed in the Padé approximant of order (3, 2) with the best-fit coefficients.

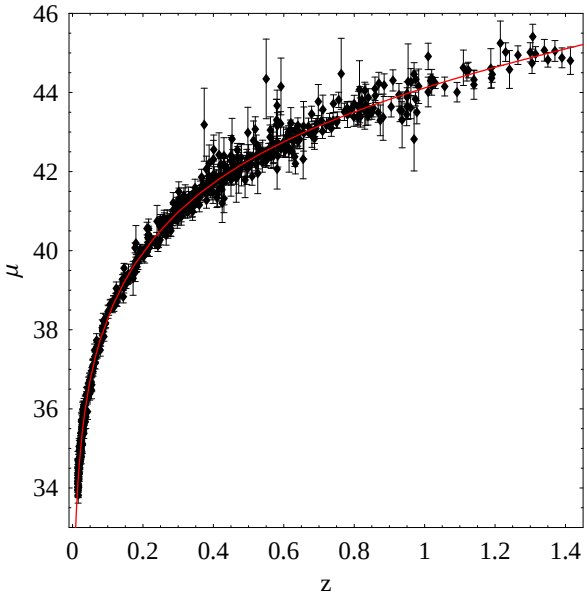

FIG. 1: The Hubble diagram of 580 Union2.1 SNIa (black diamonds) and the distance moduli expressed in the Padé approximant of order (3, 2) with the best-fit coefficients (red line).

The distance moduli of the 59 low-redshift GRBs at $z_i < 1.4$ can be directly read from the formula $\mu_{pade}(z_i)$ in Eq. (6) with the best-fit coefficients. The corresponding errors can be obtained by using the well-known error propagation equation for any quantity $Q(x_i)$ [26] (see also e.g. [27, 28])

$$\sigma^2(Q) = \sum_i^n \left(\frac{\partial Q}{\partial x_i}\right)^2_{x=\bar{x}} C_{ii} + 2\sum_{i=1}^n \sum_{j=i+1}^n \left(\frac{\partial Q}{\partial x_i}\frac{\partial Q}{\partial x_j}\right)_{x=\bar{x}} C_{ij}\,, \tag{8}$$

where C is the covariance matrix. In our case, the corresponding covariance matrix is given in Eq. (7). We plot the derived distance moduli μ and the corresponding error bars of these 59 low-redshift GRBs in the left panel of Fig. 2. In Table II, we present the numerical data of these 59 low-redshift GRBs.

As is well known, based on a sample of 12 BeppoSAX GRBs with known redshift, Amati *et al.* [29] found an empirical relation between the cosmological rest-frame spectrum peak energy $E_{\rm p,i} = E_{\rm p,obs} \times (1+z)$ and the isotropic equivalent radiated energy $E_{\rm iso}$, namely $E_{\rm p,i} = K \times E^m_{\rm iso}$. Note that the isotropic equivalent radiated energy is given by

$$E_{\rm iso} = 4\pi\, d_L^2\, S_{\rm bolo}\, (1+z)^{-1}, \tag{9}$$

GRB	z	$S_{\rm bolo}$ (10^{-5} erg cm^{-2})	$E_{\rm p,i}$ (keV)	μ
060218	0.0331	2.2 ± 0.1	4.9 ± 0.3	35.819 ± 0.017
060614	0.125	5.9 ± 2.4	55.0 ± 45.0	38.825 ± 0.014
030329	0.17	21.5 ± 3.8	100.0 ± 23.0	39.563 ± 0.013
020903	0.25	0.016 ± 0.004	3.37 ± 1.79	40.519 ± 0.013
011121	0.36	24.3 ± 6.7	1060.0 ± 265.0	41.442 ± 0.013
020819B	0.41	1.6 ± 0.4	70.0 ± 21.0	41.774 ± 0.013
050803	0.422	0.41 ± 0.09	138.0 ± 48.0	41.847 ± 0.013
990712	0.434	1.4 ± 0.3	93.0 ± 15.0	41.919 ± 0.013
010921	0.45	1.8 ± 0.2	129.0 ± 26.0	42.012 ± 0.013
091127	0.49	2.34 ± 0.28	54.0 ± 5.0	42.23 ± 0.014
081007	0.5295	0.22 ± 0.04	61.0 ± 15.0	42.43 ± 0.015
090618	0.54	28.09 ± 3.37	257.0 ± 41.0	42.48 ± 0.016
100621A	0.542	5.78 ± 0.66	146.0 ± 23.1	42.49 ± 0.016
090424	0.544	5.9 ± 1.15	273.0 ± 50.0	42.499 ± 0.016
101219B	0.55	0.76 ± 0.05	108.5 ± 12.4	42.528 ± 0.016
050223	0.5915	0.13 ± 0.02	110.0 ± 54.0	42.716 ± 0.017
050525A	0.606	2.6 ± 0.5	127.0 ± 10.0	42.779 ± 0.017
050416A	0.65	0.09 ± 0.01	25.1 ± 4.2	42.961 ± 0.018
080916	0.689	0.79 ± 0.08	184.0 ± 18.0	43.113 ± 0.018
020405	0.69	8.4 ± 0.7	354.0 ± 10.0	43.117 ± 0.018
970228	0.695	1.3 ± 0.1	195.0 ± 64.0	43.136 ± 0.019
060904B	0.703	0.28 ± 0.06	135.0 ± 41.0	43.166 ± 0.019
991208	0.706	17.2 ± 1.4	313.0 ± 31.0	43.177 ± 0.019
041006	0.716	2.3 ± 0.6	98.0 ± 20.0	43.214 ± 0.019
090328	0.736	8.93 ± 2.06	1028.0 ± 312.0	43.287 ± 0.019
030528	0.78	1.4 ± 0.2	57.0 ± 9.0	43.441 ± 0.019
051022	0.8	32.6 ± 3.1	754.0 ± 258.0	43.508 ± 0.02
100816A	0.8049	0.43 ± 0.01	246.73 ± 8.48	43.524 ± 0.02
070508	0.82	4.55 ± 1.14	378.56 ± 138.32	43.574 ± 0.02
970508	0.835	0.34 ± 0.07	145.0 ± 43.0	43.623 ± 0.02
060814	0.84	3.8 ± 0.4	473.0 ± 155.0	43.639 ± 0.02
990705	0.842	9.8 ± 1.4	459.0 ± 139.0	43.645 ± 0.02
000210	0.846	8.0 ± 0.9	753.0 ± 26.0	43.658 ± 0.02
040924	0.859	0.49 ± 0.04	102.0 ± 35.0	43.699 ± 0.02
091003	0.8969	4.75 ± 0.79	810.0 ± 157.0	43.816 ± 0.021
080319B	0.937	49.7 ± 3.8	1261.0 ± 65.0	43.936 ± 0.022
071010B	0.947	0.74 ± 0.37	101.0 ± 20.0	43.965 ± 0.023
970828	0.958	12.3 ± 1.4	586.0 ± 117.0	43.997 ± 0.023
980703	0.966	2.9 ± 0.3	503.0 ± 64.0	44.02 ± 0.024
091018	0.971	0.3 ± 0.03	55.0 ± 20.0	44.034 ± 0.024
980326	1	0.18 ± 0.04	71.0 ± 36.0	44.116 ± 0.025
021211	1.01	0.42 ± 0.05	127.0 ± 52.0	44.143 ± 0.026
991216	1.02	24.8 ± 2.5	648.0 ± 134.0	44.171 ± 0.026
080411	1.03	5.7 ± 0.3	524.0 ± 70.0	44.198 ± 0.027
000911	1.06	23.0 ± 4.7	1856.0 ± 371.0	44.279 ± 0.029
091208B	1.063	0.79 ± 0.06	255.0 ± 25.0	44.287 ± 0.029
091024	1.092	16.57 ± 1.6	586.0 ± 251.0	44.364 ± 0.031
980613	1.096	0.19 ± 0.03	194.0 ± 89.0	44.374 ± 0.032
080413B	1.1	0.73 ± 0.09	150.0 ± 30.0	44.385 ± 0.032
000418	1.12	2.8 ± 0.5	284.0 ± 21.0	44.436 ± 0.034
061126	1.1588	8.7 ± 1.0	1337.0 ± 410.0	44.535 ± 0.037
090926B	1.24	0.83 ± 0.04	204.0 ± 10.0	44.734 ± 0.046
020813	1.25	16.3 ± 4.1	590.0 ± 151.0	44.758 ± 0.047
061007	1.261	21.1 ± 2.1	890.0 ± 124.0	44.784 ± 0.048
050126A	1.29	0.17 ± 0.04	263.0 ± 110.0	44.852 ± 0.052
990506	1.3	21.7 ± 2.2	677.0 ± 156.0	44.876 ± 0.053
061121	1.314	5.1 ± 0.6	1289.0 ± 153.0	44.908 ± 0.055
071117	1.331	0.89 ± 0.21	647.0 ± 226.0	44.947 ± 0.057
100414A	1.368	15.99 ± 0.25	1486.16 ± 29.6	45.031 ± 0.062

TABLE II: The numerical data of 59 low-redshift GRBs at $z < 1.4$. The first 4 columns are taken from [16, 24], whereas the last column is derived by using Padé method. These 59 low-redshift GRBs can be used to calibrate the Amati relation. See the text for details.

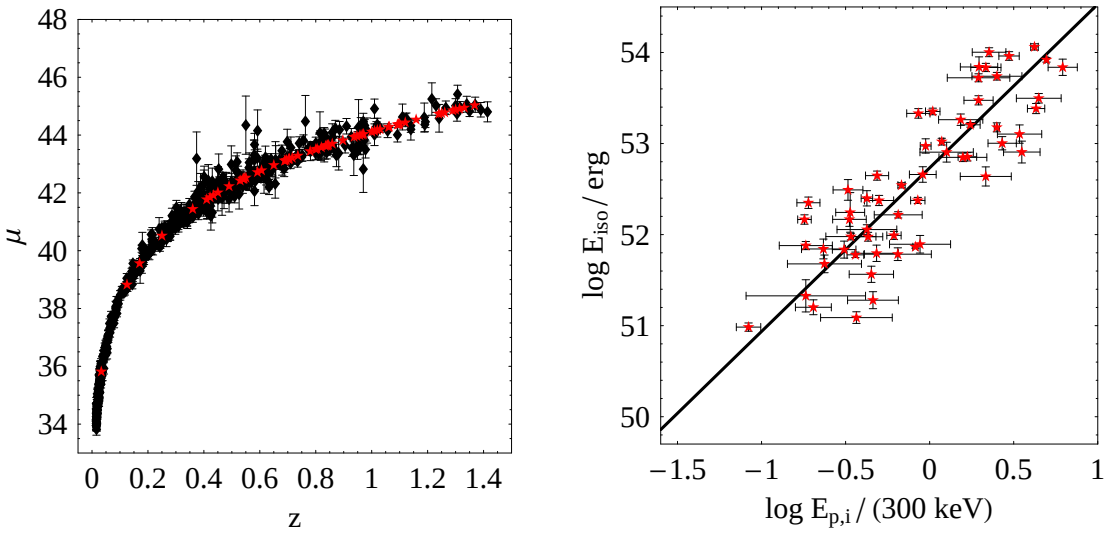

FIG. 2: Left panel: The Hubble diagram of 580 Union2.1 SNIa (black diamonds) and 59 low-redshift GRBs (red stars) whose distance moduli and errors are derived by using Padé method. Noting that the error bars of GRBs are too small, one cannot clearly see them in this panel because they are hidden by the red stars of GRBs. Right panel: 59 low-redshift GRBs data (red stars) in the $\log E_{\rm p,i}/(300\,{\rm keV}) - \log E_{\rm iso}/{\rm erg}$ plane. The best-fit calibration line is also plotted. See the text for details.

where $S_{\rm bolo}$ is the bolometric fluence of gamma rays in the GRB at redshift z, and d_L is the luminosity distance of the GRB. Following e.g. [15, 16], in this work we calibrate GRBs with the Amati relation. For convenience, following e.g. [16, 30], we recast the Amati relation as

$$\log\frac{E_{\rm iso}}{\rm erg} = \lambda + b\,\log\frac{E_{\rm p,i}}{300\,{\rm keV}}\,, \tag{10}$$

where "log" indicates the logarithm to base 10, whereas λ and b are constants to be determined. By using the well-known relation (see e.g. [1, 61, 62] for several pedagogical textbooks. Note that d_L is in units of Mpc, and m, M are the apparent magnitude and the absolute magnitude, respectively)

$$\mu \equiv m - M = 5\log\frac{d_L}{\rm Mpc} + 25\,, \tag{11}$$

we can convert the distance modulus μ of each low-redshift GRB into luminosity distance d_L (in units of Mpc), and then $E_{\rm iso}$ by employing Eq. (9) while $S_{\rm bolo}$ is known in [16, 24]. We present them in the right panel of Fig. 2, whereas $E_{\rm p,i}$ of these 59 low-redshift GRBs at $z < 1.4$ are taken from [16, 24]. From Fig. 2, one can clearly see that the intrinsic scatter is dominating over the measurement errors. Therefore, as in [14, 30], the bisector of the two ordinary least squares [31] will be used. Following the procedure of the bisector of the two ordinary least squares described in [31], we find the best fit to be

$$b = 1.7969 \qquad \text{and} \qquad \lambda = 52.7333\,, \tag{12}$$

with 1σ uncertainties

$$\sigma_b = 0.0070 \qquad \text{and} \qquad \sigma_\lambda = 0.0035\,. \tag{13}$$

The best-fit calibration line Eq. (10) with b and λ in Eq. (12) is also plotted in the right panel of Fig. 2. From Eq. (13), one can see that the calibration in this work is slightly better than the one in [15, 16].

Next, we extend the calibrated Amati relation to high redshift, namely $z > 1.4$. Since $E_{\rm p,i}$ for the 79 GRBs at $z > 1.4$ have been given in [16, 24], we can derive $E_{\rm iso}$ from the calibrated Amati relation Eq. (10) with b and λ in Eq. (12). Then, we derive the distance moduli μ for these 79 GRBs at $z > 1.4$

using Eqs. (9) and (11) while their $S_{\rm bolo}$ can be taken from [16, 24]. On the other hand, the propagated uncertainties are given by [30]

$$\sigma_\mu = \left[\left(\frac{5}{2} \sigma_{\log E_{\rm iso}} \right)^2 + \left(\frac{5}{2 \ln 10} \frac{\sigma_{S_{\rm bolo}}}{S_{\rm bolo}} \right)^2 \right]^{1/2} , \tag{14}$$

where

$$\sigma^2_{\log E_{\rm iso}} = \sigma^2_\lambda + \left(\sigma_b \log \frac{E_{\rm p,i}}{300\,{\rm keV}} \right)^2 + \left(\frac{b}{\ln 10} \frac{\sigma_{E_{\rm p,i}}}{E_{\rm p,i}} \right)^2 + \sigma^2_{E_{\rm iso,sys}} , \tag{15}$$

in which $\sigma_{E_{\rm iso,sys}}$ is the systematic error and it accounts the extra scatter of the luminosity relation. As in [30], by requiring the χ^2/dof of the 59 points at $z < 1.4$ in the $\log E_{\rm p,i}/(300\,{\rm keV}) - \log E_{\rm iso}/{\rm erg}$ plane about the best-fit calibration line to be unity, we find that

$$\sigma^2_{E_{\rm iso,sys}} = 0.1547 . \tag{16}$$

Note that in principle $\sigma^2_{E_{\rm iso,sys}}$ is a free parameter. However, if we allow it to vary with cosmology, as in e.g. [32], there might be a room for the circularity problem. Even if one does not care this problem, the constraints on cosmological models become loose, mainly due to the fact that the number of free parameters has been increased. On the other hand, we have not used any cosmology when we calibrate GRBs at $z < 1.4$, so we have no freedom to determine $\sigma^2_{E_{\rm iso,sys}}$ by cosmology, and hence we should use the method in [30] to fix it by requiring $\chi^2/dof = 1$. We admit that this prevents us to learn the systematics dominating the Amati relation. Anyway, we plot the derived distance moduli μ with 1σ uncertainties for these 79 GRBs at $z > 1.4$ in Fig. 3. We also present the numerical data of these 79 high-redshift GRBs in Table III. It is worth noting that these 79 high-redshift GRBs are obtained in a completely cosmology-independent manner, and hence can be used to constrain cosmological models without the circularity problem. We name them Mayflower sample for convenience.

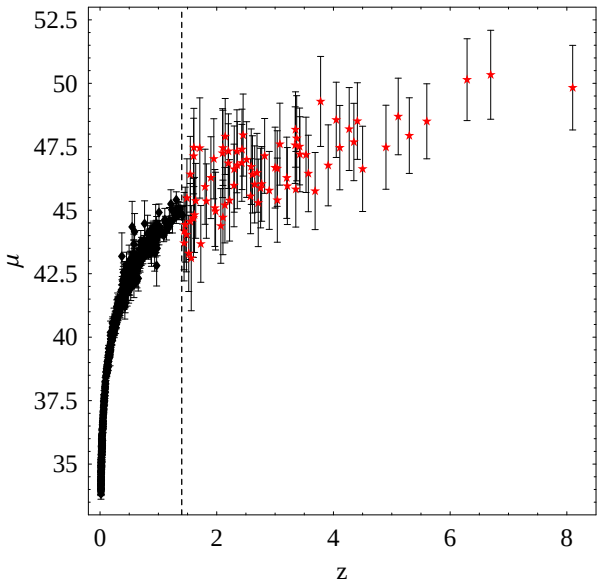

FIG. 3: The Hubble diagram of 580 Union2.1 SNIa (black diamonds) and 79 high-redshift GRBs (red stars) whose distance moduli are derived by using the calibrated Amati relation. The dashed line indicates $z = 1.4$. See the text for details.

GRB	z	$S_{\rm bolo}$ (10^{-5} erg cm^{-2})	$E_{\rm p,i}$ (keV)	μ
100814A	1.44	2.8 ± 0.09	259.616 ± 33.92	43.71 ± 1.49
050318	1.44	0.42 ± 0.03	115.0 ± 25.0	44.18 ± 1.53
110213A	1.46	1.27 ± 0.04	242.064 ± 20.91	44.43 ± 1.47
010222	1.48	14.6 ± 1.5	766.0 ± 30.0	44.04 ± 1.47
060418	1.489	2.3 ± 0.5	572.0 ± 143.0	45.48 ± 1.54
030328	1.52	6.4 ± 0.6	328.0 ± 55.0	43.3 ± 1.5
070125	1.547	13.3 ± 1.3	934.0 ± 148.0	44.56 ± 1.5
090102	1.547	3.48 ± 0.63	1149.0 ± 166.0	46.42 ± 1.49
040912	1.563	0.21 ± 0.06	44.0 ± 33.0	43.11 ± 2.07
990123	1.6	35.8 ± 5.8	1724.0 ± 466.0	44.7 ± 1.56
071003	1.604	5.32 ± 0.59	2077.0 ± 286.0	47.14 ± 1.49
090418	1.608	2.35 ± 0.59	1567.0 ± 384.0	47.48 ± 1.54
990510	1.619	2.6 ± 0.4	423.0 ± 42.0	44.82 ± 1.48
080605	1.6398	3.4 ± 0.28	650.0 ± 55.0	45.37 ± 1.47
091020	1.71	0.11 ± 0.03	280.0 ± 190.0	47.45 ± 1.97
100906A	1.727	3.91 ± 0.04	289.062 ± 55.0854	43.67 ± 1.51
080514B	1.8	2.03 ± 0.48	627.0 ± 65.0	45.93 ± 1.48
090902B	1.822	32.38 ± 1.01	2187.0 ± 31.0	45.36 ± 1.47
020127	1.9	0.38 ± 0.01	290.0 ± 100.0	46.28 ± 1.61
080319C	1.95	1.5 ± 0.3	906.0 ± 272.0	47.03 ± 1.58
081008	1.9685	0.96 ± 0.09	261.0 ± 52.0	45.09 ± 1.52
030226	1.98	1.3 ± 0.1	289.0 ± 66.0	44.97 ± 1.53
000926	2.07	2.6 ± 0.6	310.0 ± 20.0	44.38 ± 1.47
081203A	2.1	3.33 ± 0.29	1541.0 ± 757.0	47.25 ± 1.75
100728B	2.106	0.25 ± 0.01	406.886 ± 46.59	47.46 ± 1.48
090926	2.1062	15.08 ± 0.77	974.0 ± 50.0	44.72 ± 1.47
011211	2.14	0.5 ± 0.06	186.0 ± 24.0	45.2 ± 1.49
071020	2.145	0.87 ± 0.4	1013.0 ± 160.0	47.91 ± 1.5
050922C	2.198	0.47 ± 0.16	415.0 ± 111.0	46.85 ± 1.55
080804	2.2	1.01 ± 0.18	810.0 ± 45.0	47.33 ± 1.47
110205A	2.22	4.84 ± 0.52	715.0 ± 239.0	45.39 ± 1.6
060124	2.296	3.4 ± 0.5	784.0 ± 285.0	45.98 ± 1.63
021004	2.3	0.27 ± 0.04	266.0 ± 117.0	46.62 ± 1.7
051109A	2.346	0.51 ± 0.05	539.0 ± 200.0	47.32 ± 1.63
070110	2.352	0.43 ± 0.12	370.0 ± 170.0	46.78 ± 1.72
060908	2.43	0.73 ± 0.07	514.0 ± 102.0	46.87 ± 1.52
080413	2.433	0.56 ± 0.14	584.0 ± 180.0	47.4 ± 1.58
090812	2.452	3.08 ± 0.53	2000.0 ± 700.0	47.96 ± 1.62
081121	2.512	1.71 ± 0.33	871.0 ± 123.0	47.0 ± 1.49
081118	2.58	0.27 ± 0.06	147.0 ± 14.0	45.55 ± 1.48
080721	2.591	7.86 ± 1.37	1741.0 ± 227.0	46.72 ± 1.49
050820	2.612	6.4 ± 0.5	1325.0 ± 277.0	46.42 ± 1.52
030429	2.65	0.14 ± 0.02	128.0 ± 26.0	46.02 ± 1.52
080603B	2.69	0.64 ± 0.06	376.0 ± 100.0	46.48 ± 1.55
060714	2.711	0.82 ± 0.06	234.0 ± 109.0	45.29 ± 1.72
091029	2.752	0.47 ± 0.04	230.0 ± 66.0	45.87 ± 1.57
081222	2.77	1.67 ± 0.17	505.0 ± 34.0	46.04 ± 1.47
050603	2.821	3.5 ± 0.2	1333.0 ± 107.0	47.14 ± 1.47
050401	2.9	1.9 ± 0.4	467.0 ± 110.0	45.78 ± 1.54
090715B	3	1.09 ± 0.17	536.0 ± 172.0	46.68 ± 1.59
080607	3.036	8.96 ± 0.48	1691.0 ± 226.0	46.65 ± 1.49
081028	3.038	0.81 ± 0.1	234.0 ± 93.0	45.4 ± 1.66
060607A	3.082	0.54 ± 0.08	575.0 ± 200.0	47.61 ± 1.61
020124	3.2	1.2 ± 0.1	448.0 ± 148.0	46.28 ± 1.6
060526	3.21	0.12 ± 0.06	105.0 ± 21.0	45.95 ± 1.52
050908	3.344	0.09 ± 0.01	195.0 ± 36.0	47.57 ± 1.51
080810	3.35	1.82 ± 0.2	1470.0 ± 180.0	48.18 ± 1.48
061222B	3.355	0.44 ± 0.07	200.0 ± 28.0	45.83 ± 1.49
030323	3.37	0.12 ± 0.04	270.0 ± 113.0	47.84 ± 1.68
971214	3.42	0.87 ± 0.11	685.0 ± 133.0	47.51 ± 1.51
060707	3.425	0.23 ± 0.04	279.0 ± 28.0	47.21 ± 1.48
060115	3.53	0.25 ± 0.04	285.0 ± 34.0	47.18 ± 1.48
090323	3.57	14.98 ± 1.83	1901.0 ± 343.0	46.45 ± 1.51
060906	3.686	0.55 ± 0.06	209.0 ± 43.0	45.76 ± 1.52
060605	3.78	0.1 ± 0.02	490.0 ± 251.0	49.29 ± 1.77
060210	3.91	1.4 ± 0.19	575.0 ± 186.0	46.77 ± 1.59
060206	4.048	0.14 ± 0.03	394.0 ± 46.0	48.56 ± 1.48
090516	4.109	1.96 ± 0.38	971.0 ± 390.0	47.47 ± 1.66
050505	4.27	0.52 ± 0.08	661.0 ± 245.0	48.2 ± 1.63
080916C	4.35	10.13 ± 2.13	2646.0 ± 566.0	47.69 ± 1.52
060223A	4.41	0.12 ± 0.02	339.0 ± 63.0	48.51 ± 1.51
000131	4.5	4.7 ± 0.8	987.0 ± 416.0	46.63 ± 1.68
060510B	4.9	0.87 ± 0.07	575.0 ± 227.0	47.48 ± 1.65
060522	5.11	0.17 ± 0.03	427.0 ± 79.0	48.7 ± 1.51
050814	5.3	0.24 ± 0.05	339.0 ± 47.0	47.94 ± 1.49
060927	5.6	0.27 ± 0.04	475.0 ± 47.0	48.51 ± 1.48
050904	6.29	2.0 ± 0.2	3178.0 ± 1094.0	50.15 ± 1.61
080913	6.695	0.12 ± 0.03	710.0 ± 350.0	50.34 ± 1.75
090423	8.1	0.12 ± 0.03	491.0 ± 200.0	49.83 ± 1.67

TABLE III: The numerical data of 79 calibrated GRBs at $z > 1.4$. The first 4 columns are taken from [16, 24], whereas the last column is derived by using the calibrated Amati relation. These 79 calibrated GRBs are named Mayflower sample, and can be used to constrain cosmological models without the circularity problem.

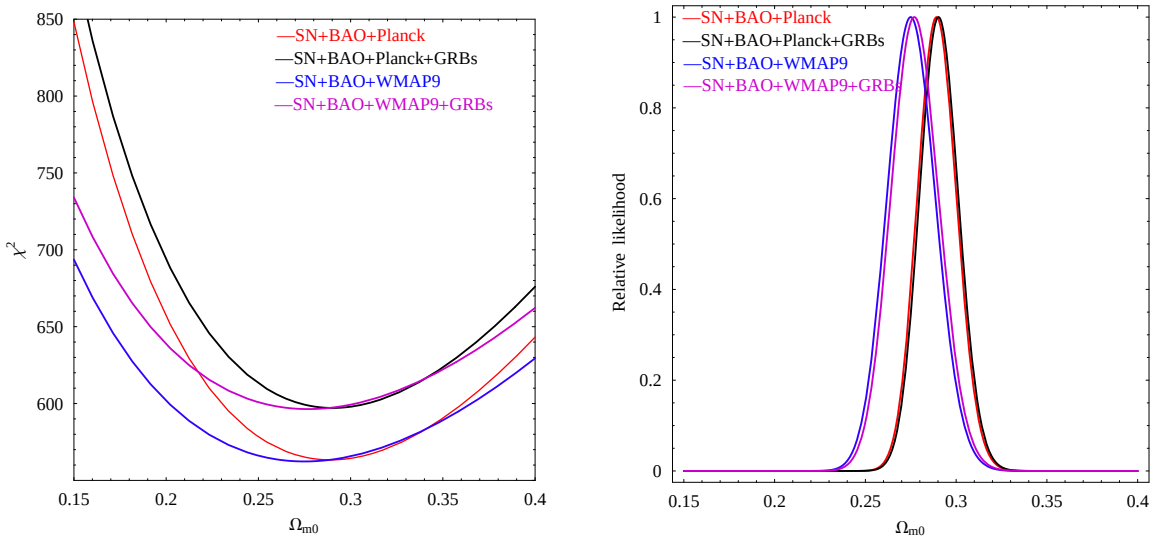

FIG. 4: The χ^2 and likelihood $\mathcal{L} \propto e^{-\chi^2/2}$ as functions of Ω_{m0} from various joint datasets for the ΛCDM model.

III. OBSERVATIONAL CONSTRAINTS ON COSMOLOGICAL MODELS

In this section, we consider the observational constraints on various cosmological models. In addition to the 79 Mayflower GRBs obtained in the present work (see Table III), we also consider other types of observational data. Of course, the Union2.1 SNIa dataset [25] (which consists of 580 SNIa) will be used. The data ponits of both SNIa and GRBs are given in terms of the distance modulus. Following the methodology described in e.g. [16] (especially, see the discussions between Eqs. (9)—(13) of [16] and note that H_0 has been marginalized), one can obtain the corresponding $\chi^2_{\rm SN}$ and $\chi^2_{\rm GRBs}$, respectively. Another important probe is the cosmic microwave background (CMB) anisotropy [33, 34]. Recently, the WMAP Collaboration released their final 9-year data (WMAP9) [33]. The Planck Collaboration also released their data (Planck) [34]. As is noted by Planck Collaboration itself, there is a subtle tension between Planck data and WMAP data. So, in this work we consider these two CMB data separately. However, using the full data of CMB to perform a global fitting consumes a large amount of computation time and power. As an alternative, one can instead use the shift parameter R from CMB data. It is argued in e.g. [35–37] that it is model-independent and contains the main information of the full CMB data. The shift parameter R is defined by [35–37]

$$R \equiv \Omega_{m0}^{1/2} \int_0^{z_*} \frac{d\tilde{z}}{E(\tilde{z})}\,, \tag{17}$$

where Ω_{m0} is the present fractional density of pressureless matter; z_* is the redshift of recombination; $E \equiv H/H_0$ and H is the Hubble parameter (the subscript "0" indicates the present value of corresponding quantity). Its was determined in [35] that $R = 1.7302 \pm 0.0169$ and $z_* = 1089.09$ for WMAP9 [33], whereas $R = 1.7499 \pm 0.0088$ and $z_* = 1090.41$ for Planck [34]. The corresponding $\chi^2_{\rm CMB} = (R - R_{obs})^2/\sigma_R^2$. Finally, we consider also the observation of large-scale structure (LSS) [38]. Similarly, it is also argued in e.g. [36] that the distance parameter A from the baryon acoustic oscillation (BAO) peak is model-independent and contains the main information of the LSS data. The distance parameter A is defined by [38, 39]

$$A \equiv \Omega_{m0}^{1/2} E(z_b)^{-1/3} \left[\frac{1}{z_b} \int_0^{z_b} \frac{d\tilde{z}}{E(\tilde{z})}\right]^{2/3}, \tag{18}$$

where $z_b = 0.35$. In [39], the value of A has been determined to be $0.469\,(n_s/0.98)^{-0.35} \pm 0.017$. Here the scalar spectral index n_s is taken to be 0.9662 [37] from the Planck data [34]. The corresponding

	ΛCDM Model		XCDM Model		
	χ^2_{min}/dof	Ω_{m0}	χ^2_{min}/dof	Ω_{m0}	$w_{\rm x}$
SN+BAO+Planck	563.352/581	$0.2892^{+0.0109}_{-0.0106}\,(1\sigma)\,^{+0.0222}_{-0.0208}\,(2\sigma)$	562.645/580	0.2874	-1.0326
SN+BAO+Planck+GRBs	597.135/660	$0.2903^{+0.0109}_{-0.0106}\,(1\sigma)\,^{+0.0221}_{-0.0208}\,(2\sigma)$	596.545/659	0.2887	-1.0300
SN+BAO+WMAP9	562.325/581	$0.2750^{+0.0135}_{-0.0131}\,(1\sigma)\,^{+0.0275}_{-0.0257}\,(2\sigma)$	562.278/580	0.2742	-0.9900
SN+BAO+WMAP9+GRBs	596.396/660	$0.2770^{+0.0135}_{-0.0130}\,(1\sigma)\,^{+0.0274}_{-0.0256}\,(2\sigma)$	596.333/659	0.2761	-0.9883

TABLE IV: The χ^2_{min} and the best-fit model parameters from various joint datasets for the ΛCDM, XCDM models, respectively. Note that the 1σ and 2σ uncertainties are also given for the ΛCDM model.

$\chi^2_{\rm BAO}=(A-A_{obs})^2/\sigma_A^2$. Thus, the total χ^2 is given by $\chi^2=\chi^2_{\rm SN}+\chi^2_{\rm BAO}+\chi^2_{\rm CMB}+\chi^2_{\rm GRBs}$. The best-fit model parameters are determined by minimizing the total χ^2. As in [41, 42], the 68.3% confidence level is determined by $\Delta\chi^2\equiv\chi^2-\chi^2_{min}\leq 1.0$, 2.3, 3.53, 4.72 for $n_p=1$, 2, 3, 4 respectively, where n_p is the number of free model parameters. Similarly, the 95.4% confidence level is determined by $\Delta\chi^2\equiv\chi^2-\chi^2_{min}\leq 4.0$, 6.18, 8.02, 9.72 for $n_p=1$, 2, 3, 4, respectively.

In the following subsections, we use various datasets to constrain cosmological models. To see the possible difference between Planck and WMAP9, we constrain the models with these two CMB data separately. We also consider the datasets with or without 79 Mayflower GRBs, to see the effect of GRBs on the constraints. So, in the followings, we use four joint datasets, namely, SN+BAO+Planck, SN+BAO+Planck+GRBs, SN+BAO+WMAP9, SN+BAO+WMAP9+GRBs, respectively. Note that we consider a flat Friedmann-Robertson-Walker (FRW) universe containing only pressureless matter and dark energy, except the case of Dvali-Gabadadze-Porrati (DGP) model in which the cosmic acceleration is due to a modification to general relativity rather than dark energy.

A. ΛCDM model

At first, we consider the observational constraints on the flat ΛCDM model. As is well known, the corresponding $E=H/H_0$ reads

$$E(z)=\sqrt{\Omega_{m0}(1+z)^3+(1-\Omega_{m0})}\,. \tag{19}$$

It is easy to obtain the total χ^2 as a function of the single model parameter Ω_{m0} for the ΛCDM model. We present the corresponding χ^2 and likelihood $\mathcal{L}\propto e^{-\chi^2/2}$ in Fig. 4. In Table IV, the χ^2_{min} and the best-fit model parameter Ω_{m0} (with 1σ and 2σ uncertainties) from various joint datasets are given. From Fig. 4 and Table IV, we can see that Planck data favors a larger Ω_{m0} than WMAP9 data, while GRBs data also favors a slightly larger Ω_{m0}.

B. XCDM model

In the XCDM model, the equation-of-state parameter (EoS) of dark energy is a constant $w_{\rm x}$. The corresponding $E(z)$ is given by

$$E(z)=\sqrt{\Omega_{m0}(1+z)^3+(1-\Omega_{m0})(1+z)^{3(1+w_{\rm x})}}\,. \tag{20}$$

There are two free model parameters, namely Ω_{m0} and $w_{\rm x}$. By minimizing the corresponding total χ^2, we find the best-fit parameters and present them in Table IV. In Fig. 5, we present the corresponding 68.3% and 95.4% confidence level contours in the $\Omega_{m0}-w_{\rm x}$ parameter space from various joint datasets for the XCDM model. From Fig. 5 and Table IV, it is easy to see that Planck data favors a larger Ω_{m0} and a smaller $w_{\rm x}$ than WMAP9 data, while GRBs data favors slightly larger values of both Ω_{m0} and $w_{\rm x}$.

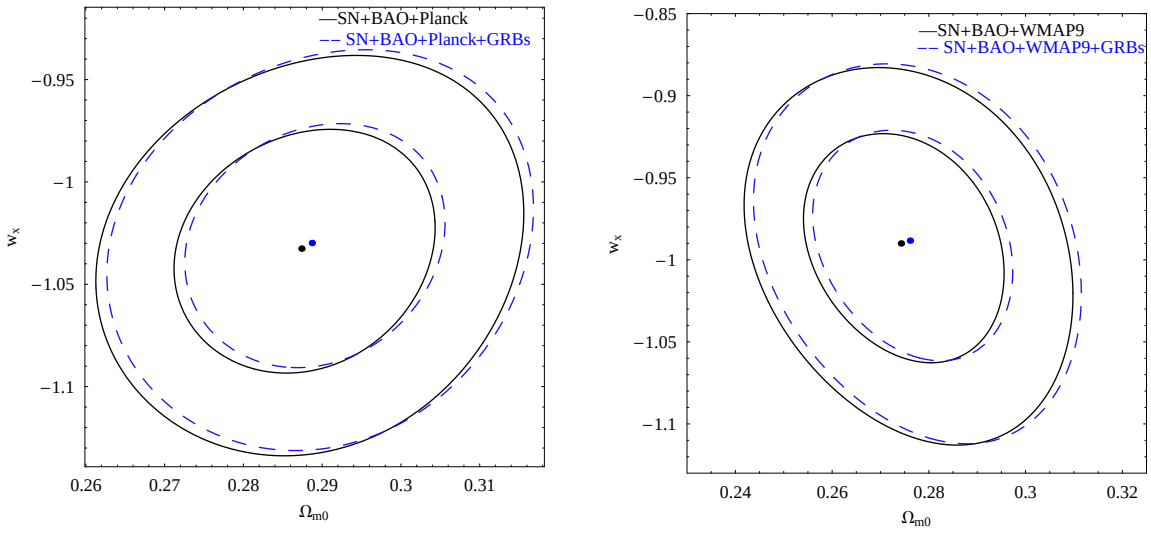

FIG. 5: The 68.3% and 95.4% confidence level contours in the $\Omega_{m0} - w_{\rm x}$ parameter space from various joint datasets for the XCDM model. The best-fit parameters are indicated by a solid point.

	χ^2_{min}	χ^2_{min}/dof	Ω_{m0}	w_0	w_a
SN+BAO+Planck	562.445	0.971	0.2847	−0.9775	−0.2782
SN+BAO+Planck+GRBs	596.480	0.907	0.2872	−0.9988	−0.1551
SN+BAO+WMAP9	562.235	0.971	0.2750	−1.0143	0.1301
SN+BAO+WMAP9+GRBs	596.159	0.906	0.2776	−1.0363	0.2546

TABLE V: The χ^2_{min} and the best-fit model parameters from various joint datasets for the CPL model.

C. CPL model

In the well-known Chevallier-Polarski-Linder (CPL) model [40], the EoS of dark energy is given by

$$w_{de} = w_0 + w_a(1-a) = w_0 + w_a\frac{z}{1+z}\,, \tag{21}$$

where a is scale factor; w_0 and w_a are both constants. The corresponding $E(z)$ is given by [41, 42]

$$E(z) = \left[\Omega_{m0}(1+z)^3 + (1-\Omega_{m0})\,(1+z)^{3(1+w_0+w_a)}\exp\left(-\frac{3w_a z}{1+z}\right)\right]^{1/2}. \tag{22}$$

There are three free parameters in this model, namely Ω_{m0}, w_0 and w_a. By minimizing the corresponding total χ^2, we find the best-fit model parameters from various joint datasets for the CPL model, and present them in Table V. In Figs. 6, 7 and 8, we also show the 68.3% and 95.4% confidence level contours in the $w_0 - w_a$, $\Omega_{m0} - w_0$ and $\Omega_{m0} - w_a$ planes, respectively. From Table V and Figs. 6–8, we see that Planck data favors a larger Ω_{m0}, a larger w_0 and a smaller w_a than WMAP9 data. Note that Planck data favors a $w_0 > -1$ and a negative w_a, which means that dark energy was phantom-like ($w_{de} < -1$) in the past, then its EoS crossed the phantom divide, and became quintessence-like ($w_{de} > -1$) recently; finally its

EoS will become positive in the future. On the contrary, WMAP9 data favors a $w_0 < -1$ and a positive w_a, which means that dark energy was quintessence-like ($w_{de} > -1$) in the past, then its EoS crossed the phantom divide, and became phantom-like ($w_{de} < -1$) recently; finally the universe will end in a big rip. On the other hand, we find that GRBs data favors a slightly larger Ω_{m0}, a slightly smaller w_0 and a slightly larger w_a.

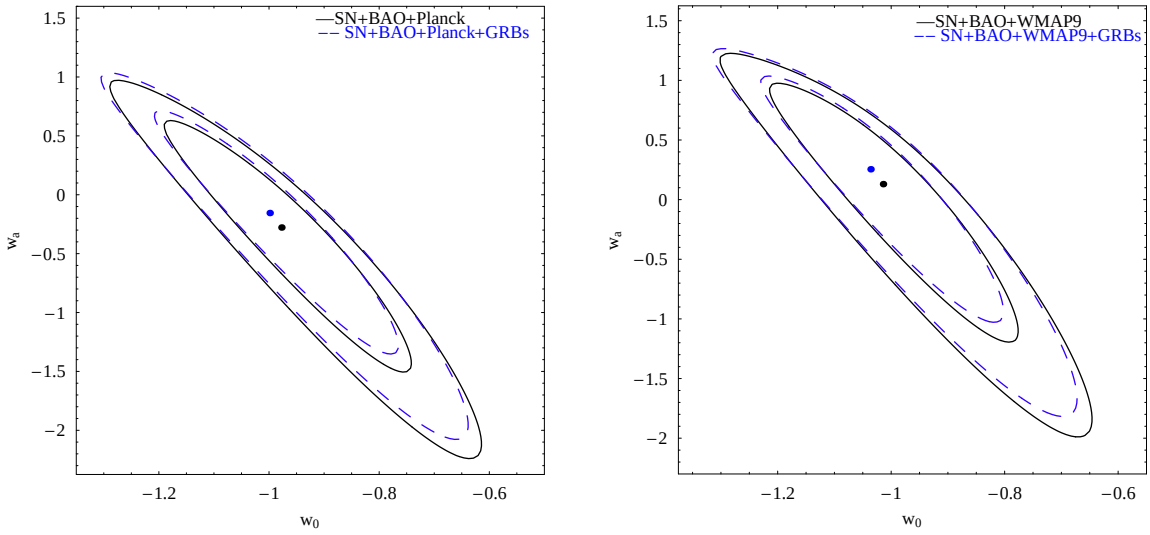

FIG. 6: The 68.3% and 95.4% confidence level contours in the $w_0 - w_a$ plane from various joint datasets for the CPL model. The best-fit parameters are indicated by a solid point.

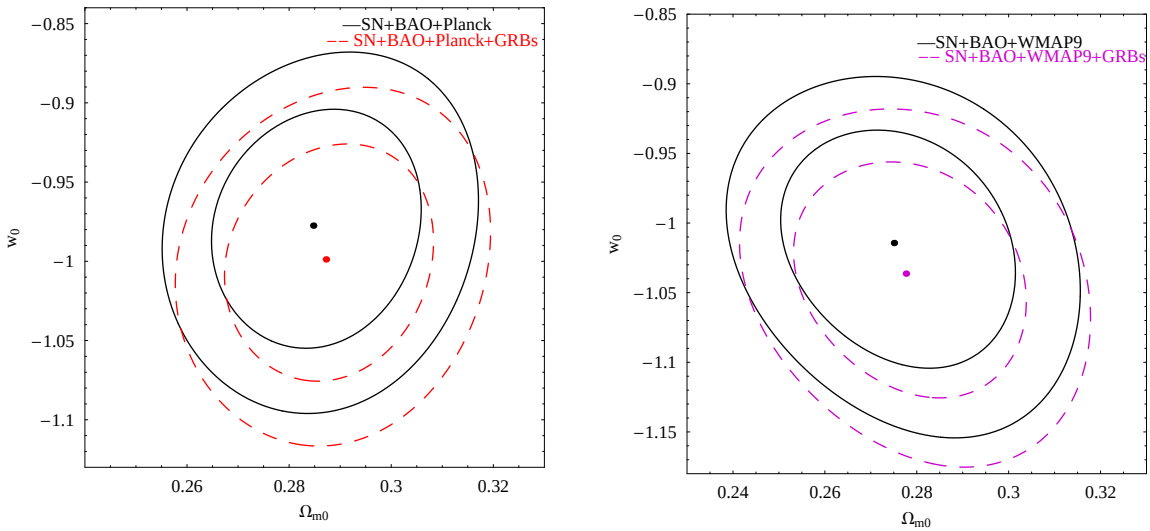

FIG. 7: The same as in Fig. 6, except for the $\Omega_{m0} - w_0$ plane.

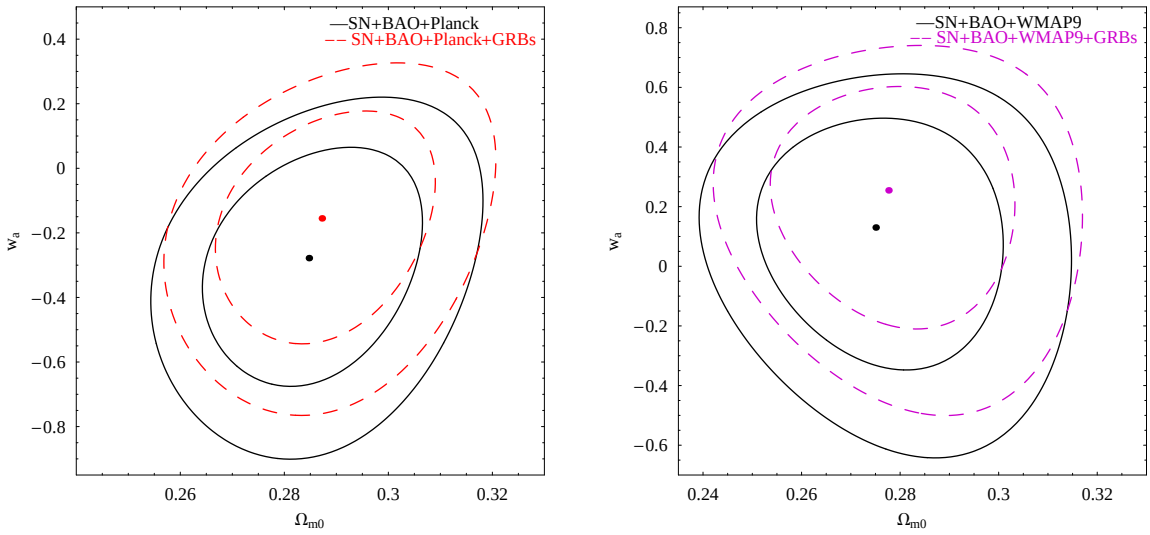

FIG. 8: The same as in Fig. 6, except for the $\Omega_{m0} - w_a$ plane.

D. DGP model

The Dvali-Gabadadze-Porrati (DGP) model is a popular model which modifies the gravity to allow the cosmic acceleration without dark energy [43, 44]. This model could arise from the braneworld theory in which gravity leaks out into the bulk on large scales. As is well known, for the flat DGP model (here we only consider the self-accelerating branch), the corresponding $E(z)$ is given by [43, 44]

$$E(z) = \sqrt{\Omega_{m0}(1+z)^3 + \Omega_{rc}} + \sqrt{\Omega_{rc}}\,, \tag{23}$$

where Ω_{rc} is a constant. It is easy to see that $E(z=0) = 1$ requires

$$\Omega_{m0} = 1 - 2\sqrt{\Omega_{rc}}\,. \tag{24}$$

Therefore, the DGP model has only one independent model parameter Ω_{rc}. Notice that $0 \leq \Omega_{rc} \leq 1/4$ is required by $0 \leq \Omega_{m0} \leq 1$. It is easy to obtain the total χ^2 as a function of the single model parameter Ω_{rc}. In Fig. 9, we plot the corresponding χ^2 and likelihood $\mathcal{L} \propto e^{-\chi^2/2}$ from various joint datasets for the DGP model. In Table VI, we also present the χ^2_{min} and the best-fit model parameters (with 1σ and 2σ uncertainties) from various joint datasets for the DGP model. It is easy to see that Planck data favors a smaller Ω_{rc} than WMAP9 data, while GRBs data favors a slightly smaller Ω_{rc}.

	χ^2_{min}	χ^2_{min}/dof	Ω_{rc}
SN+BAO+Planck	665.697	1.146	$0.1092^{+0.0038}_{-0.0038}\ (1\sigma)\ ^{+0.0075}_{-0.0077}\ (2\sigma)$
SN+BAO+Planck+GRBs	698.435	1.058	$0.1092^{+0.0038}_{-0.0038}\ (1\sigma)\ ^{+0.0075}_{-0.0077}\ (2\sigma)$
SN+BAO+WMAP9	611.705	1.053	$0.1339^{+0.0047}_{-0.0048}\ (1\sigma)\ ^{+0.0092}_{-0.0096}\ (2\sigma)$
SN+BAO+WMAP9+GRBs	644.750	0.977	$0.1336^{+0.0046}_{-0.0047}\ (1\sigma)\ ^{+0.0092}_{-0.0096}\ (2\sigma)$

TABLE VI: The χ^2_{min} and the best-fit model parameters (with 1σ and 2σ uncertainties) from various joint datasets for the DGP model.

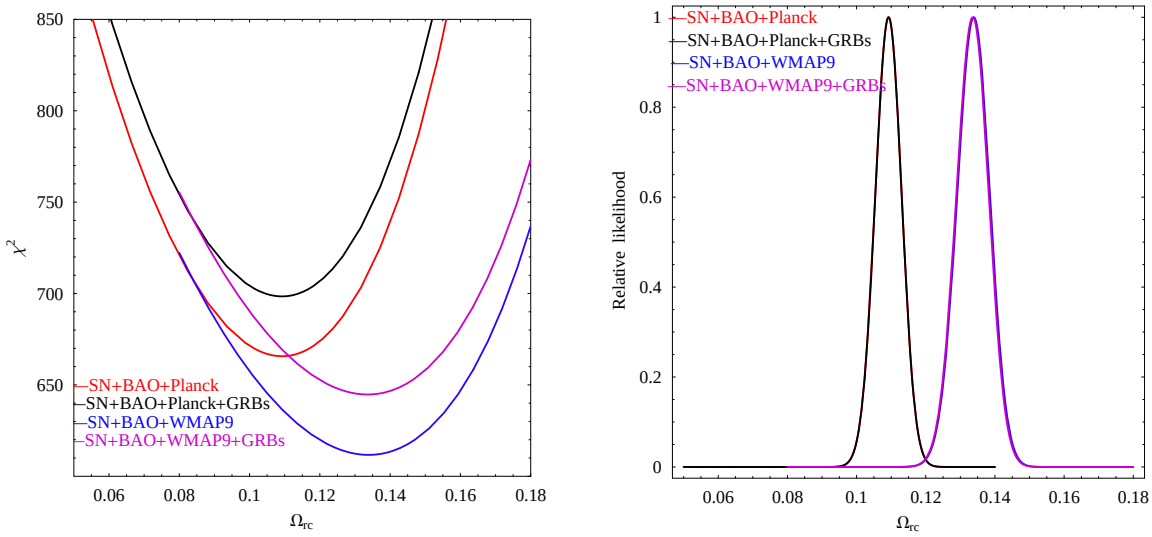

FIG. 9: The χ^2 and likelihood $\mathcal{L} \propto e^{-\chi^2/2}$ as functions of Ω_{rc} from various joint datasets for the DGP model.

E. SGCG model

The Chaplygin gas (CG) model was firstly proposed by Kamenshchik *et al.* [45]. In this model, the pressure p of the fluid is related to its energy density ρ through $p = -\mathcal{A}/\rho$, where $\mathcal{A}$ is a positive constant. In the literature, the generalized Chaplygin gas model (GCG) [46] model is extensively considered, in which the equation of state for this fluid is generalized to

$$p = -\mathcal{A}/\rho^{\eta}\,, \tag{25}$$

where η is a constant. Originally, the CG or GCG models were considered as promising models united dark matter and dark energy [45, 46], since this fluid can mimic pressureless matter in the early time and cosmological constant in the late time. However, this possibility was excluded later (see e.g. [55]). Thus, in the literature, the CG or GCG are usually considered as a candidate of dark energy only, coexisting with dark matter.

In the GCG model, there are 3 free parameters, namely Ω_{m0}, η and $\mathcal{A}$. In [47], Lima *et al.* proposed a simplified GCG (SGCG) model, in which they argued that the parameter $\mathcal{A}$ could be related with η according to $\mathcal{A} = \eta\rho_0^{1+\eta}$. So, the simplified equation of state becomes [47, 48]

$$p = -\eta\rho_0 \left(\frac{\rho_0}{\rho}\right)^{\eta}\,. \tag{26}$$

As is argued in [47], $\eta > 0$ is required by $p < 0$ to accelerate the universe, while $\eta \leq 1$ is required by the causality, namely the adiabatic sound speed of this fluid cannot exceed the speed of light. So, as in e.g. [47–50], we also restrict $0 < \eta \leq 1$ in this work. In the SGCG model, the corresponding $E(z)$ is given by [47–49]

$$E(z) = \left\{\Omega_{m0}(1+z)^3 + (1-\Omega_{m0})\left[(1-\eta)(1+z)^{3(1+\eta)} + \eta\right]^{1/(1+\eta)}\right\}^{1/2}\,. \tag{27}$$

Now, there are only two free parameters in this model, namely Ω_{m0} and η. By minimizing the corresponding total χ^2, we find the best-fit parameters and present them in Table VII. In Fig. 10, we present the corresponding 68.3% and 95.4% confidence level contours in the $\Omega_{m0} - \eta$ parameter space from various joint datasets for the SGCG model. From Table VII and Fig. 10, it is easy to see that Plank data favors

	χ^2_{min}	χ^2_{min}/dof	Ω_{m0}	η
SN+BAO+Planck	563.352	0.971	0.2892	1.0
SN+BAO+Planck+GRBs	597.135	1.068	0.2903	1.0
SN+BAO+WMAP9	562.227	0.969	0.2773	0.99996
SN+BAO+WMAP9+GRBs	596.233	0.905	0.2799	0.99994

TABLE VII: The χ^2_{min} and the best-fit model parameters from various joint datasets for the SGCG model.

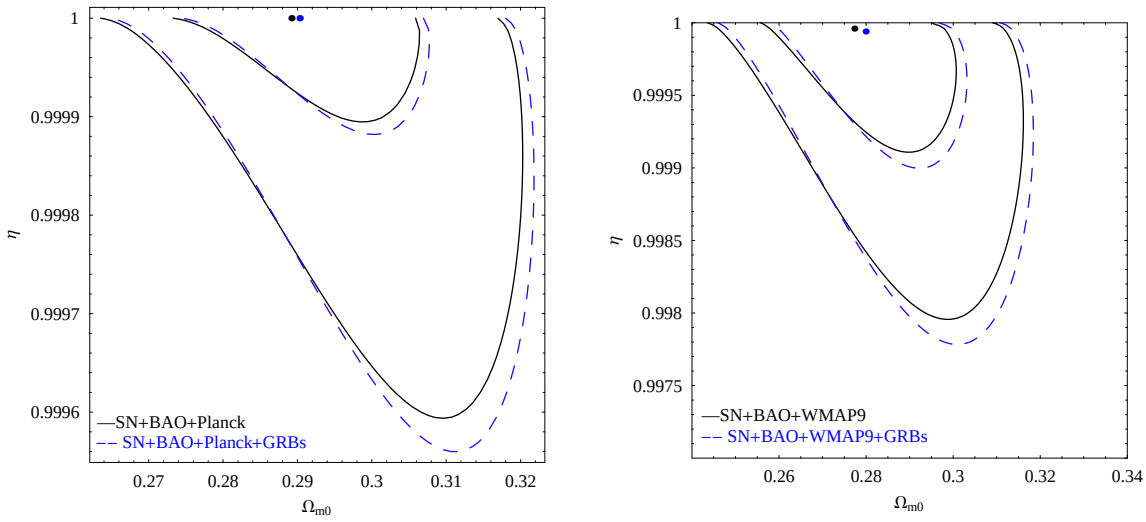

FIG. 10: The 68.3% and 95.4% confidence level contours in the $\Omega_{m0} - \eta$ parameter space from various joint datasets for the SGCG model. The best-fit parameters are indicated by a solid point.

a larger Ω_{m0} and a slightly larger η than WMAP9 data, while GRBs data favors a slightly larger Ω_{m0} and a slightly smaller η. However, it is obvious that all joint datasets favor $\eta \simeq 1$ (in this case the SGCG model reduces to the original CG model).

F. RDE model

The so-called holographic dark energy (HDE) has been studied extensively in the literature. Based on the holographic principle, it is argued that the density of dark energy is given by $\rho_{de} = 3c^2 M_p^2 L^{-2}$, where M_p is the reduced Planck mass; c is a numerical constant characterizing some uncertainties in the effective quantum field theory, and L is the IR cut-off. In [51], Gao *et al.* proposed the so-called Ricci dark energy (RDE) model, which can be regarded as a variant of HDE model. In this model, the IR cut-off L is chosen to be proportional to the Ricci scalar curvature radius, and hence $L^{-2} \propto \dot{H} + 2H^2$. So, the density of RDE reads [51]

$$\rho_{de} = 3\alpha M_p^2 \left(\dot{H} + 2H^2\right) , \tag{28}$$

where α is a dimensionless constant. In this model, it is easy to find that [51, 52]

$$E(z) = \left[\frac{2\Omega_{m0}}{2-\alpha} (1+z)^3 + \left(1 - \frac{2\Omega_{m0}}{2-\alpha}\right) (1+z)^{4-2/\alpha} \right]^{1/2} . \tag{29}$$

	χ^2_{min}	χ^2_{min}/dof	Ω_{m0}	α
SN+BAO+Planck	615.549	1.061	0.3734	0.2993
SN+BAO+Planck+GRBs	648.474	0.984	0.3734	0.2993
SN+BAO+WMAP9	589.919	1.017	0.3305	0.3514
SN+BAO+WMAP9+GRBs	622.894	0.945	0.3310	0.3514

TABLE VIII: The χ^2_{min} and the best-fit model parameters from various joint datasets for the RDE model.

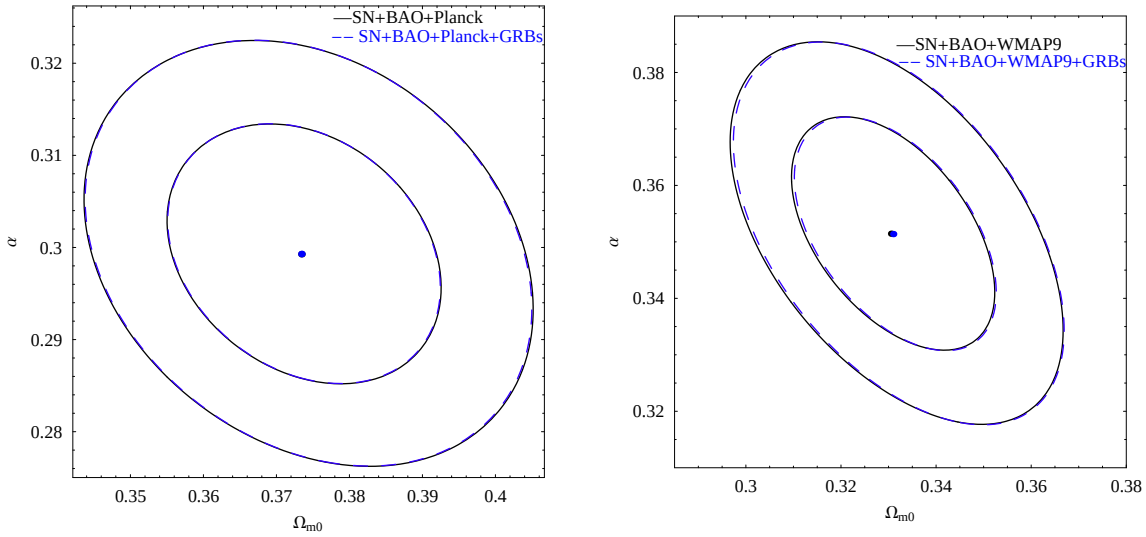

FIG. 11: The 68.3% and 95.4% confidence level contours in the $\Omega_{m0} - \alpha$ parameter space from various joint datasets for the RDE model. The best-fit parameters are indicated by a solid point.

There are two free model parameters, namely Ω_{m0} and α. By minimizing the corresponding total χ^2, we find the best-fit parameters and present them in Table VIII. In Fig. 11, we present the corresponding 68.3% and 95.4% confidence level contours in the $\Omega_{m0} - \alpha$ parameter space from various joint datasets for the RDE model. From Table VIII and Fig. 11, we see that Plank data favors a larger Ω_{m0} and a smaller α, while GRBs data favors a slightly larger Ω_{m0}. However, it is obvious that the effect of GRBs data on the constraints is fairly weak for the RDE model.

IV. CONCLUSION AND DISCUSSIONS

Gamma-ray bursts (GRBs) are among the most powerful sources in the universe. In the recent years, GRBs have been proposed as a complementary probe to type Ia supernovae (SNIa). However, as is well known, there is a circularity problem in the use of GRBs to study cosmology. In this work, based on the Padé approximant, we propose a new cosmology-independent method to calibrate GRBs. We consider a sample consisting of 138 long Swift GRBs and obtain 79 calibrated long GRBs at high-redshift $z > 1.4$ (named Mayflower sample) which can be used to constrain cosmological models without the circularity problem. Then, we consider the constraints on several cosmological models with these 79 calibrated GRBs and other observational data. We show that GRBs are competent to be a complementary probe to the other well-established cosmological observations.

Some remarks are in order. First, in our calibration of GRBs, the Padé approximant plays an important role. In fact, the present work is not the first one using the Padé approximant in cosmology. We refer to e.g. [23, 56, 59] for the previous relevant works. In these works, the Padé approximant has been used in the slow-roll inflation, the reconstruction of the scalar field potential from SNIa, the data fitting of luminosity distance, the EoS parameterization, and the cosmological perturbation in LSS.

Second, when we calculate the errors for the distance moduli of the 59 low-redshift GRBs at $z_i < 1.4$, the standard error propagation equation is used. In fact, there is an alternative way. Similar to e.g. [28], we can instead use the Monte Carlo method to evaluate the error propagations. That is, we generate a multivariate Gaussian distribution from the best-fit parameters and the corresponding covariance matrix. And then, we randomly sample N suits (say, $N = 10^6$) of the parameters $\{\alpha_0, \alpha_1, \alpha_2, \alpha_3, \beta_1, \beta_2\}$ from this distribution. For each suit of $\{\alpha_0, \alpha_1, \alpha_2, \alpha_3, \beta_1, \beta_2\}$, we can find the corresponding distance moduli of the 59 low-redshift GRBs from Eq. (6). After all, we can determine the means and the corresponding 1σ errors for the distance moduli of the 59 low-redshift GRBs at $z_i < 1.4$ from these N samples. Of course, it is not surprising that the errors for the distance moduli of the 59 low-redshift GRBs obtained from the standard error propagation equation and the Monte Carlo method are coincident.

Third, we admit that the validity of the Amati relation is still in debate (we thank the referee for pointing out this issue). While many works support the Amati relation, it has also been seriously challenged in the literature (see e.g. [63, 64]). In particular, it is argued in e.g. [64] that there exists a significant problem in using the Amati Relation for cosmological purposes. Therefore, one should be careful and keep this issue in mind when using the Amati Relation in cosmology.

Fourth, the Mayflower sample of 79 calibrated GRBs obtained in the present work can be used to constrain cosmological models without the circularity problem. In this work, we have shown that GRBs are competent to be a complementary probe to the other well-established cosmological observations. However, as is shown in Sec. III, the inclusion of GRBs cannot considerably improve the constraints on most of the cosmological models (in fact, the constraints on some models become even worse). Therefore, to make GRBs into a competitively cosmological probe, one should accumulate more and more GRBs with smaller and smaller errors. We hope this could be done in the near future.

Finally, it is worth noting that when we fit the Union2.1 SNIa dataset [25], the numerical data given in [65] are used (see e.g. Eqs. (3), (7), and Sec. III). Actually, this is equivalent to use the diagonal covariance matrix without systematics given in [66]. As is shown in e.g. [25], this diagonal covariance matrix without systematics might lead to an under-estimation of the errors (we thank the referee for pointing out this issue). To avoid this, we should use instead the full covariance matrix with systematics given in [67]. However, we choose not to redo all of the analysis with the full covariance matrix. As mentioned above, the inclusion of GRBs cannot considerably improve the constraints on most of the cosmological models (in fact, the constraints on some models become even worse), mainly due to the large errors of the current GRBs sample. If we redo all of the analysis with the full covariance matrix, this status cannot be changed and the constraints will become even worse, since the errors of GRBs coming from the full covariance matrix are larger. Noting that our main goal of this work is just to show that GRBs are competent to be a complementary probe to the other well-established cosmological observations, the conclusion will not be changed with using the full covariance matrix. In this sense, redoing all of the analysis with the full covariance matrix makes no significant difference. Nevertheless, we would like to remind the readers to be aware of this issue when using the Mayflower sample of 79 calibrated GRBs in the relevant works.

ACKNOWLEDGEMENTS

We thank the anonymous referee for quite useful comments and suggestions, which helped us to improve this work. We are grateful to Minzi Feng, as well as Zu-Cheng Chen, Xiao-Peng Yan, Ya-Nan Zhou, Xiao-Bo Zou, Hong-Yu Li, Shou-Long Li, and Dong-Ze Xue, for kind help and discussions. This work was supported in part by NSFC under Grants No. 11175016 and No. 10905005, as well as NCET under Grant No. NCET-11-0790.

[1] A. G. Riess *et al.*, Astron. J. **116**, 1009 (1998) [astro-ph/9805201];
S. Perlmutter *et al.*, Astrophys. J. **517**, 565 (1999) [astro-ph/9812133].
[2] G. Ghirlanda, G. Ghisellini and C. Firmani, New. J. Phys. **8**, 123 (2006) [astro-ph/0610248].
[3] B. Zhang, Chin. J. Astron. Astrophys. **7**, 1 (2007) [astro-ph/0701520];
B. Zhang, astro-ph/0611774.
[4] P. Meszaros, Rept. Prog. Phys. **69**, 2259 (2006) [astro-ph/0605208];
V. Bromm and A. Loeb, arXiv:0706.2445;
S. E. Woosley and J. S. Bloom, Ann. Rev. Astron. Astrophys. **44**, 507 (2006) [astro-ph/0609142].
[5] B. E. Schaefer, Astrophys. J. **660**, 16 (2007) [astro-ph/0612285].
[6] R. Salvaterra *et al.*, Nature **461**, 1258 (2009).
[7] A. Cucchiara *et al.*, Astrophys. J. **743**, 154 (2011) [arXiv:1107.3352].
[8] A. G. Riess *et al.*, Astrophys. J. **659**, 98 (2007) [astro-ph/0611572].
[9] Z. G. Dai, E. W. Liang and D. Xu, Astrophys. J. **612**, L101 (2004) [astro-ph/0407497].
[10] G. Ghirlanda, G. Ghisellini, D. Lazzati and C. Firmani, Astrophys. J. **613**, L13 (2004) [astro-ph/0408350].
[11] E. W. Liang and B. Zhang, Astrophys. J. **633**, 611 (2005) [astro-ph/0504404].
[12] C. Firmani *et al.*, Mon. Not. Roy. Astron. Soc. **360**, L1 (2005) [astro-ph/0501395].
[13] H. Li *et al.*, Astrophys. J. **680**, 92 (2008) [arXiv:0711.1792].
[14] N. Liang, W. K. Xiao, Y. Liu and S. N. Zhang, Astrophys. J. **685**, 354 (2008) [arXiv:0802.4262];
N. Liang and S. N. Zhang, AIP Conf. Proc. **1065**, 367 (2008) [arXiv:0808.2655].
[15] H. Wei and S. N. Zhang, Eur. Phys. J. C **63**, 139 (2009) [arXiv:0808.2240].
[16] H. Wei, JCAP **1008**, 020 (2010) [arXiv:1004.4951].
[17] Y. Kodama *et al.*, Mon. Not. Roy. Astron. Soc. **391**, L1 (2008) [arXiv:0802.3428].
[18] S. Capozziello and L. Izzo, Astron. Astrophys, **490**, 31 (2008) [arXiv:0806.1120];
S. Capozziello and L. Izzo, Astron. Astrophys, **519**, A73 (2010) [arXiv:1003.5319];
V. F. Cardone, M. Perillo and S. Capozziello, Mon. Not. Roy. Astron. Soc. **417**, 1672 (2011) [arXiv:1105.1122].
[19] H. Gao, N. Liang and Z. H. Zhu, Int. J. Mod. Phys. D **21**, 1250016 (2012) [arXiv:1003.5755].
[20] Y. Wang, Phys. Rev. D **78**, 123532 (2008) [arXiv:0809.0657].
[21] L. X. Xu, JCAP **1204**, 025 (2012) [arXiv:1005.5055].
[22] H. Padé, Ann. Sci. Ecole Norm. Sup., **9** (3), 1-93 (1892);
S. G. Krantz and H. R. Parks, *A primer of real analytic functions*, Birkhäuser (1992);
G. A. Baker, Jr. and P. Graves-Morris, *Padé Approximants*, Cambridge University Press (1996);
http://en.wikipedia.org/wiki/Pade_approximant
http://www.scholarpedia.org/article/Pade_approximant
http://www-sop.inria.fr/apics/anap03/PadeTalk.pdf
[23] M. Adachi and M. Kasai, Prog. Theor. Phys. **127**, 145 (2012) [arXiv:1111.6396];
H. Wei, X. P. Yan and Y. N. Zhou, JCAP **1401**, 045 (2014) [arXiv:1312.1117].
[24] Y. P. Qin and Z. F. Chen, Mon. Not. Roy. Astron. Soc. **430**, 163 (2013) [arXiv:1311.4713].
[25] N. Suzuki *et al.* [SCP Collaboration], Astrophys. J. **746**, 85 (2012) [arXiv:1105.3470];
The numerical data of the full Union2.1 sample are available at http://supernova.lbl.gov/Union
[26] U. Alam, V. Sahni, T. D. Saini and A. A. Starobinsky, astro-ph/0406672.
[27] U. Alam *et al.*, Mon. Not. Roy. Astron. Soc. **354**, 275 (2004) [astro-ph/0311364].
[28] H. Wei, N. N. Tang and S. N. Zhang, Phys. Rev. D **75**, 043009 (2007) [astro-ph/0612746].
[29] L. Amati *et al.*, Astron. Astrophys. **390**, 81 (2002) [astro-ph/0205230].
[30] B. E. Schaefer, Astrophys. J. **660**, 16 (2007) [astro-ph/0612285].
[31] T. Isobe, E. D. Feigelson, M. G. Akritas and G. J. Babu, Astrophys. J. **364**, 104 (1990).
[32] S. Basilakos and L. Perivolaropoulos, Mon. Not. Roy. Astron. Soc. **391**, 411 (2008) [arXiv:0805.0875].
[33] G. Hinshaw *et al.* [WMAP Collaboration], Astrophys. J. Suppl. **208**, 19 (2013) [arXiv:1212.5226].
[34] P. A. R. Ade *et al.* [Planck Collaboration], Astron. Astrophys. **571**, A16 (2014) [arXiv:1303.5076].
[35] D. L. Shafer and D. Huterer, Phys. Rev. D **89**, 063510 (2014) [arXiv:1312.1688].
[36] Y. Wang and P. Mukherjee, Astrophys. J. **650**, 1 (2006) [astro-ph/0604051];
J. R. Bond, G. Efstathiou and M. Tegmark, Mon. Not. Roy. Astron. Soc. **291**, L33 (1997) [astro-ph/9702100].
[37] Y. Wang and S. Wang, Phys. Rev. D **88**, 043522 (2013) [arXiv:1304.4514].
[38] M. Tegmark *et al.* [SDSS Collaboration], Phys. Rev. D **69**, 103501 (2004) [astro-ph/0310723];
M. Tegmark *et al.* [SDSS Collaboration], Astrophys. J. **606**, 702 (2004) [astro-ph/0310725];
U. Seljak *et al.* [SDSS Collaboration], Phys. Rev. D **71**, 103515 (2005) [astro-ph/0407372];
M. Tegmark *et al.* [SDSS Collaboration], Phys. Rev. D **74**, 123507 (2006) [astro-ph/0608632].
[39] D. J. Eisenstein *et al.* [SDSS Collaboration], Astrophys. J. **633**, 560 (2005) [astro-ph/0501171].

[40] M. Chevallier and D. Polarski, Int. J. Mod. Phys. D **10**, 213 (2001) [gr-qc/0009008];
E. V. Linder, Phys. Rev. Lett. **90**, 091301 (2003) [astro-ph/0208512].
[41] S. Nesseris and L. Perivolaropoulos, Phys. Rev. D **70**, 043531 (2004) [astro-ph/0401556].
[42] R. Lazkoz, S. Nesseris and L. Perivolaropoulos, JCAP **0511**, 010 (2005) [astro-ph/0503230].
[43] G. R. Dvali, G. Gabadadze and M. Porrati, Phys. Lett. B **485**, 208 (2000) [hep-th/0005016].
[44] C. Deffayet, Phys. Lett. B **502**, 199 (2001) [hep-th/0010186];
C. Deffayet, G. R. Dvali and G. Gabadadze, Phys. Rev. D **65**, 044023 (2002) [astro-ph/0105068].
[45] A. Y. Kamenshchik, U. Moschella and V. Pasquier, Phys. Lett. B **511**, 265 (2001) [gr-qc/0103004].
[46] M. C. Bento, O. Bertolami and A. A. Sen, Phys. Rev. D **66**, 043507 (2002) [gr-qc/0202064].
[47] J. A. S. Lima, J. V. Cunha and J. S. Alcaniz, Astropart. Phys. **30**, 196 (2008) [astro-ph/0608469].
[48] J. A. S. Lima, J. V. Cunha and J. S. Alcaniz, Astropart. Phys. **31**, 233 (2009) [astro-ph/0611007].
[49] S. M. Dong and P. X. Wu, Chin. Phys. Lett. **24**, 1782 (2007).
[50] J. S. Alcaniz, D. Jain and A. Dev, Phys. Rev. D **67**, 043514 (2003) [astro-ph/0210476].
[51] C. Gao, F. Q. Wu, X. Chen and Y. G. Shen, Phys. Rev. D 79, 043511 (2009) [arXiv:0712.1394].
[52] M. Li, X. D. Li, S. Wang and X. Zhang, JCAP **0906**, 036 (2009) [arXiv:0904.0928].
[53] G. Schwarz, Ann. Stat. **6**, 461 (1978).
[54] H. Akaike, IEEE Trans. Automatic Control **19**, 716 (1974).
[55] H. Sandvik, M. Tegmark, M. Zaldarriaga and I. Waga, Phys. Rev. D **69**, 123524 (2004) [astro-ph/0212114].
[56] A. R. Liddle, P. Parsons and J. D. Barrow, Phys. Rev. D **50**, 7222 (1994) [astro-ph/9408015];
A. Yoshisato, T. Matsubara and M. Morikawa, Astrophys. J. **498**, 48 (1998) [astro-ph/9707296];
T. D. Saini *et al.*, Phys. Rev. Lett. **85**, 1162 (2000) [astro-ph/9910231];
D. Huterer and M. S. Turner, Phys. Rev. D **64**, 123527 (2001) [astro-ph/0012510];
J. Jonsson, A. Goobar, R. Amanullah and L. Bergstrom, JCAP **0409**, 007 (2004) [astro-ph/0404468];
D. Blas, M. Garny and T. Konstandin, JCAP **1401**, 010 (2014) [arXiv:1309.3308];
C. Gruber and O. Luongo, Phys. Rev. D **89**, 103506 (2014) [arXiv:1309.3215].
[57] Z. Cano, Astrophys. J. **794**, 121 (2014) [arXiv:1407.2589];
Z. Cano and P. Jakobsson, arXiv:1409.3570 [astro-ph.CO];
A. I. Bogomazov, V. M. Lipunov, and A. V. Tutukov, Astron. Rept. **51**, 308 (2007);
J. J. Wei, X. F. Wu and F. Melia, Astrophys. J. **772**, 43 (2013) [arXiv:1301.0894].
[58] A. Aviles, C. Gruber, O. Luongo and H. Quevedo, Phys. Rev. D **86**, 123516 (2012) [arXiv:1204.2007];
S. Capozziello, M. De Laurentis and O. Luongo, Annalen Phys. **526**, 309 (2014) [arXiv:1406.6996].
[59] A. Aviles, A. Bravetti, S. Capozziello and O. Luongo, Phys. Rev. D **90**, 043531 (2014) [arXiv:1405.6935].
[60] N. Gehrels *et al.* [Swift Science Collaboration], Astrophys. J. **611**, 1005 (2004) [astro-ph/0405233];
D. N. Burrows *et al.*, Space Sci. Rev. **120**, 165 (2005) [astro-ph/0508071];
P. W. A. Roming *et al.*, Space Sci. Rev. **120**, 95 (2005) [astro-ph/0507413];
N. Gehrels *et al.*, Ann. Rev. Astron. Astrophys. **47**, 567 (2009) [arXiv:0909.1531];
T. Sakamoto *et al.*, Astrophys. J. Suppl. **175**, 179 (2008) [arXiv:0707.4626];
T. Sakamoto *et al.*, Astrophys. J. Suppl. **195**, 2 (2011) [arXiv:1104.4689];
http://swift.gsfc.nasa.gov
[61] S. Weinberg, *Cosmology*, Oxford University Press (2008).
[62] D. W. Hogg, astro-ph/9905116;
J. Christiansen and A. Siver, Am. J. Phys. **80**, 367 (2012) [arXiv:1204.0039].
[63] N. R. Butler, D. Kocevski and J. S. Bloom, Astrophys. J. **694**, 76 (2009) [arXiv:0802.3396];
A. Shahmoradi and R. J. Nemiroff, Mon. Not. Roy. Astron. Soc. **411**, 1843 (2011) [arXiv:0904.1464].
[64] A. C. Collazzi, B. E. Schaefer, A. Goldstein and R. D. Preece, Astrophys. J. **747**, 39 (2012) [arXiv:1112.4347].
[65] http://supernova.lbl.gov/Union/figures/SCPUnion2.1_mu_vs_z.txt
[66] http://supernova.lbl.gov/Union/figures/SCPUnion2.1_covmat_nosys.txt
[67] http://supernova.lbl.gov/Union/figures/SCPUnion2.1_covmat_sys.txt